PHYSICAL REVIEW A VOLUME 25, NUMBER 4 APRIL 1982

Oscillatory free-induction decay and oscillatory spin echoes

M. Kunitomo
College of Liberal Arts, Kobe University, Kobe, Japan 657

T. Endo, S. Nakanishi, and T. Hashi
Department of Physics, Kyoto University, Kyoto, Japan 606

(Received 17 August 1981)

Oscillatory free-induction decay (FID) theoretically predicted by Schenzle, Wong, and Brewer was observed by using NMR in an inhomogeneously broadened proton system. Oscillatory behaviors were also observed, in the same system, in two-pulse echoes generated by large-area pulses. These phenomena appear in a highly inhomogeneous-broadened atomic or spin two-level system driven by resonant laser or rf pulses with areas equal to or larger than 2π. Detailed studies were made for spin-locked and notched echoes. Behaviors of the oscillatory FID and the oscillatory echoes were theoretically examined by solving the Bloch equations and numerically integrating the solution over the inhomogeneous broadening. Excellent agreement between experiment and theory was obtained. Analytic expressions for the shapes of the locked- and notched-type echoes are obtained, which interpret the main characteristics of these echoes, when the infinite linewidth of the inhomogeneous broadening and the δ-function-type excitation for one of the pulses are assumed.

I. INTRODUCTION

The oscillatory behavior of the free-induction decay (FID) was theoretically predicted by Schenzle, Wong and Brewer (SWB)[1] for atomic or spin two-level systems excited by a laser or a radio-frequency (rf) resonant field in the form of a square pulse, when the following conditions are satisfied: (1) the inhomogeneous linewidth is very large compared with the homogeneous one, (2) the pulse area is equal to or larger than 2π, and (3) the magnitude of the driving field is smaller than the inhomogeneous linewidth. They derived their results by solving the Bloch equations and numerically integrating the solution over the inhomogeneous broadening. They also obtained an analytic expression for the oscillatory FID, which is approximate but interprets the main characteristics well.

The first decisive experimental verification of the oscillatory FID was made by us,[2] using an inhomogeneously broadened proton NMR system. Later we observed the oscillatory FID in the optical region in ruby.[3] The "edge-echo" effect observed by Bloom[4] in his classical experiment in 1955 is attributed to the oscillatory FID.

Physically, the oscillation of FID can be interpreted as the sideband effect[1]: The laser or the rf driving field directly excites only a part of the inhomogeneously broadened spectrum because the field intensity is smaller than the inhomogeneous linewidth. However, resonant dipoles nutate around the driving field and create sidebands, which excite other parts of the spectrum. Hence, the resultant radiation after the pulse contains many frequency components giving rise to the oscillation of FID.

A part of this paper is concerned with the detailed description of the NMR experiment confirming the oscillatory behavior of FID.

In connection with the oscillatory FID, it is expected that two-pulse echoes display similar oscillations (oscillatory echoes) when the pulse areas are large. This was pointed out by SWB, and ESR experiments and calculations by Mims[5] in 1966 provided examples of this phenomenon. However, as far as treating cases where both pulse areas are large, we obtain very complicated echo shapes and, in general, no uniform oscillation of echoes as in the case of FID.

In the present paper, we treat rather simplified cases where only one of the pulses is a large-area one. In these cases echo patterns become relatively

simple. Moreover, analytic expressions of the echo shapes can be obtained in a manner similar to that in the FID cases,[1] when the width of the inhomogeneous broadening is assumed to be infinite. When the first pulse is short and the area of the second is large, the echoes obtained are called "spin-locked echoes"[6] in NMR or "radiation-locked echoes"[7] in optical region. When the area of the first pulse is large and the second is short, the echoes obtained are called "notched echoes"[8] according to the naming in optical regions.

Theoretical and experimental investigations described below show that echoes exhibit amplitude oscillations, when the area of the longer pulse is equal to or larger than 2π, and the conditions (1) and (3), as in the case of FID, are satisfied. These oscillations have not been recognized so far except for our latest observation of oscillatory radiation-locked echoes.[5] A part of multiple spin echoes observed by us (M.K. and T.H.)[8] are considered to be a special case of these echoes.

The theory of the oscillatory echoes is developed in a manner similar to that of FID, i.e., by solving the Bloch equations and numerically integrating the solution over the inhomogeneous broadening. The results are applicable to both NMR and optical-resonance experiments.

In this work, the experimental verification of the oscillatory FID and the oscillatory echoes were done by using NMR. The utility of NMR comes from the fact that a highly monochromatic excitation field (rf field) is available and experimental conditions, such as shapes of the pulses, pulse areas, the width of the inhomogeneous broadening, and so on, can be easily and accurately controlled. In addition, the long homogeneous decay time of nuclear spins enables us to observe the full signals and to analyze them without the consideration of the relaxation effects. The agreement between theoretical predictions and experimental results is quite excellent, as shown in Sec. III.

II. THEORETICAL ANALYSIS

A. Basic equations

We start from the Bloch equations for a magnetic moment $\vec{m}$ in a reference frame rotating around the static magnetic field $\vec{H}_0$ (z direction) at a frequecy Ω of the applied rf field $\vec{H}_1$. Relaxation effects are neglected in accordance with the experimental conditions. When the direction of the rf field $\vec{H}_1$ is taken along the x axis in this frame, the Bloch equations can be written as

$$\begin{aligned} dm_x/dt &= \Delta m_y \ , \\ dm_y/dt &= -\Delta m_x + \chi m_z \ , \\ dm_z/dt &= -\chi m_y \ , \end{aligned} \tag{1}$$

where Δ and χ are the frequency offset and Rabi frequency defined by $\gamma H_0 - \Omega$ and γH_1, respectively, and γ is the gyromagnetic ratio. General solutions of the coupled differential equations are

$$\begin{aligned} m_x(t) &= k_1\chi + k_2\Delta\cos\beta t - k_3\Delta\sin\beta t \ , \\ m_y(t) &= -k_2\beta\sin\beta t - k_3\beta\cos\beta t \ , \\ m_z(t) &= k_1\Delta - k_2\chi\cos\beta t + k_3\chi\sin\beta t \ , \end{aligned} \tag{2}$$

where

$$\beta = (\Delta^2+\chi^2)^{1/2} \ .$$

When the initial conditions are

$$m_x(0) = m_{x0} \ ,$$

$$m_y(0) = m_{y0} \ ,$$

and

$$m_z(0) = m_{z0} \ ,$$

the coefficients k_1, k_2, and k_3 become

$$\begin{aligned} k_1 &= (\chi m_{x0} + \Delta m_{z0})/\beta^2 \ , \\ k_2 &= (\Delta m_{x0} - \chi m_{z0})/\beta^2 \ , \\ k_3 &= -m_{y0}/\beta \ . \end{aligned} \tag{3}$$

In the absence of the rf field the time development of the moment can be obtained by setting $\chi = 0$ in (2) and (3) as

$$\begin{aligned} m_x(t) &= m_{x0}\cos\Delta t + m_{y0}\sin\Delta t \ , \\ m_y(t) &= -m_{x0}\sin\Delta t + m_{y0}\cos\Delta t \ , \\ m_z(t) &= m_{z0} \ . \end{aligned} \tag{4}$$

The response of the moment to any pulse sequences can be obtained by combining Eqs. (2) and (4). The solutions $m_x(t)$ and $m_y(t)$ must be integrated over the inhomogeneous line-shape function $g(\Delta)$ to obtain dispersion and absorption signals as

$$\begin{aligned} u(t) &= \int_{-\infty}^{+\infty} m_x(t) g(\Delta) d\Delta \ , \\ v(t) &= \int_{-\infty}^{+\infty} m_y(t) g(\Delta) d\Delta \ . \end{aligned} \tag{5}$$

In the following calculations the line-shape function $g(\Delta)$ is assumed to be the Gaussian as

$$g(\Delta)=\frac{N}{\sqrt{\pi}\sigma^*}e^{-(\Delta/\sigma^*)^2}, \tag{6}$$

where σ^* is the inhomogeneous linewidth full width at half maximum (FWHM) and N the spin number density.

B. Free-induction decay

The theory of oscillatory FID was already given by SWB. The formulas given in this section are essentially the same as those by SWB. Suppose that a square pulse with duration τ_1 is applied at $t=0$ to the system. When the initial conditions are

$$m_x(0)=0\,,$$

$$m_y(0)=0\,,$$

and

$$m_z(0)=m_0\,,$$

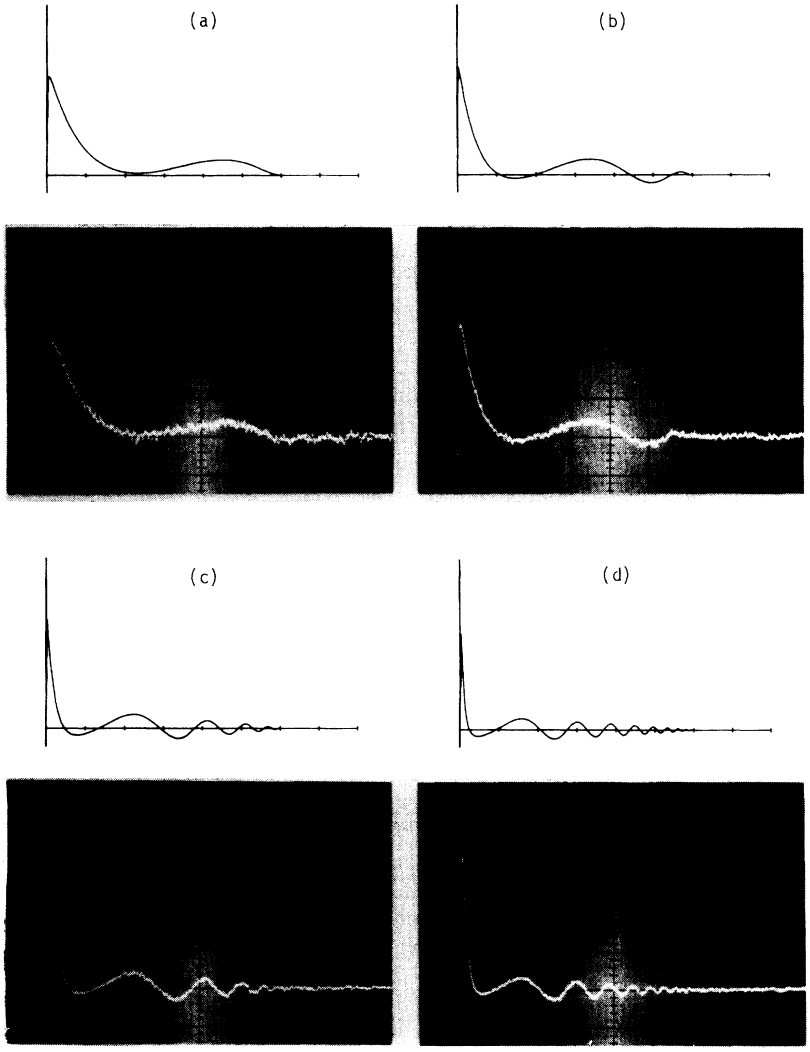

FIG. 1. Calculated and observed shapes of oscillatory FID signals for pulse area 2π, 4π, 10π, and 20π [from (a) to (d)]. The horizontal scale is 100 μs/div.

the time developments of $m_x(t)$ and $m_y(t)$ after the pulse can be obtained as

$$m_x(t)=(m_0\chi/\beta^2)[\Delta(1-\cos\beta\tau_1)\cos\Delta(t-\tau_1)+\beta\sin\beta\tau_1\sin\Delta(t-\tau_1)]\ ,$$
$$m_y(t)=(m_0\chi/\beta^2)[-\Delta(1-\cos\beta\tau_1)\sin\Delta(t-\tau_1)+\beta\sin\beta\tau_1\cos\Delta(t-\tau_1)]\ . \tag{7}$$

Although the notations are different, the solution $m_y(t)$ is the same as $v(t)$ of SWB [Eq. (2.14) in Ref.1] except for the relaxation terms. The FID signal (the v-mode signal) is obtained by inserting $m_y(t)$ into the second equation of (5). Since $m_x(t)$ is an odd function of Δ, the u-mode signal given by the first equation of (5) vanishes when the line-shape function is symmetric about the line center. However, if the line-shape function is asymmetric with respect to Δ, as in the present experiment (see Sec. III), the u-mode signal appears.

Generally the integral (5) cannot be carried out analytically. Therefore, we performed numerical calculations to obtain theoretical shapes of FID. The results of the numerical calculations for pulse areas $\chi\tau_1 = 2n\pi$ (n = 1,2,5,10,15,20) and $(2n+1)\pi$ (n =1,2,7) are shown in Figs. 1–3. The values of the parameter used are

$$\sigma^*=2\pi\times 85.2\times 10^3 \text{ rad/s}$$

and τ_1= 0.6 ms. The FID shapes for pulse areas 2π, 4π, 10π, and 20π were already obtained by SWB. Our results coincide with theirs.

When the linewidth σ^* is assumed to be infinite, an analytic form of Eq. (5) can be obtained by using the Laplace transform method. Here we reproduce the formula given by SWB as

$$v(t)=\begin{cases}0, & t>2\tau_1\\ -\pi m_0\chi^2 g(0)\displaystyle\int_{t-\tau_1}^{\tau_1}\left[\frac{s-(t-\tau_1)}{s+(t-\tau_1)}\right]^{1/2} J_1\{\chi[s^2-(t-\tau_1)^2]^{1/2}\}ds, & \tau_1<t<2\tau_1\end{cases} \tag{8}$$

where J_1 is the Bessel function of order 1. Equation (8) shows that the oscillatory FID lasts only for a times τ_1 after the pulse and no signal is expected after that.

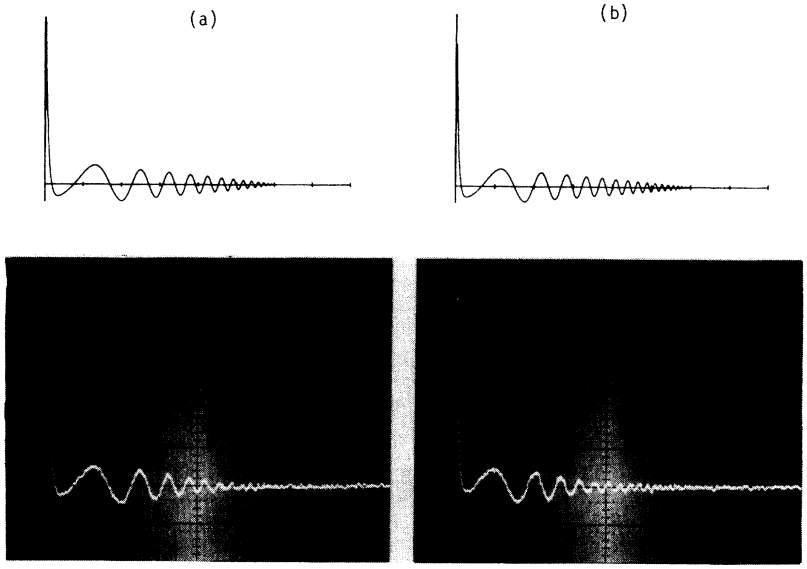

FIG. 2. Calculated and observed shapes of oscillatory FID signals for pulse area (a) 30π and (b) 40π. The horizontal scale is 100 μs/div.

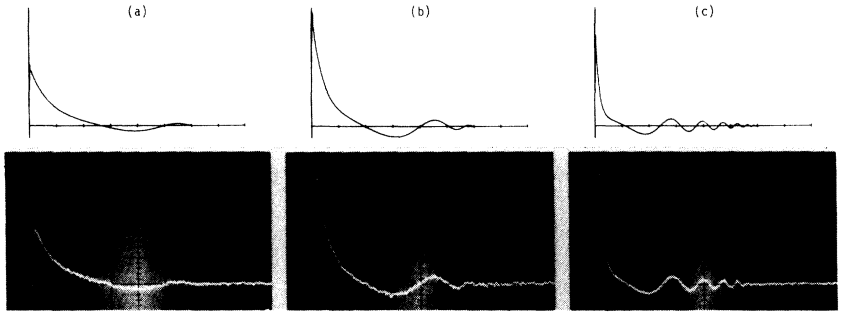

FIG. 3. Calculated and observed shapes of oscillatory FID signals for pulse area 3π, 5π, and 15π [from (a) to (c)]. The horizontal scale is 100 μs/div.

C. Two-pulse echoes

We treat a case where, as shown in Fig. 4, the second pulse with duration τ_2 is applied at $t=\tau_1+\tau$ after the application of the first pulse with duration τ_1 at $t=0$. The time development of the moment after the second pulse can be obtained by successive applications of Eqs. (2) and (4). The calculation is straightforward and a somewhat lengthy result for $m_y(t)$ is obtained as

$$
\begin{aligned}
m_y/m_0=&(\chi/\beta^4)(-\Delta(\Delta^2+\chi^2\cos\beta\tau_1)(1-\cos\beta\tau_2)\sin\Delta(t-\tau_1-\tau-\tau_2)\\
&+\beta(\Delta^2+\chi^2\cos\beta\tau_1)\sin\beta\tau_2\cos\Delta(t-\tau_1-\tau-\tau_2)\\
&-\tfrac{1}{2}\Delta\{(1-\cos\beta\tau_1)[\chi^2+(2\Delta^2+\chi^2)\cos\beta\tau_2]+\beta^2\sin\beta\tau_1\sin\beta\tau_2\}\sin\Delta(t-\tau_1-\tau_2)\\
&-\tfrac{1}{2}\beta\{\sin\beta\tau_1[\chi^2-(2\Delta^2+\chi^2)\cos\beta\tau_2]+2\Delta^2(1-\cos\beta\tau_1)\sin\beta\tau_2\}\cos\Delta(t-\tau_1-\tau_2)\\
&-\tfrac{1}{2}\chi^2\Delta(1-\cos\beta\tau_1)(1-\cos\beta\tau_2)\sin\Delta(t-\tau_1-2\tau-\tau_2)\\
&-\tfrac{1}{2}\chi^2\beta\sin\beta\tau_1(1-\cos\beta\tau_2)\cos\Delta(t-\tau_1-2\tau-\tau_2))\,,
\end{aligned}
\tag{9}
$$

where the same initial conditions as in the previous section are assumed at $t=0$ and the amplitudes of the two pulses are assumed to be equal. The first two terms containing the factors

$$\sin(t-\tau_1-\tau-\tau_2)$$

and

$$\cos(t-\tau_1-\tau-\tau_2)$$

give FID after the second pulse, and the last two terms containing

$$\sin(t-\tau_1-2\tau-\tau_2)$$

and

$$\cos(t-\tau_1-2\tau-\tau_2)$$

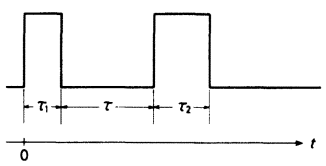

FIG. 4. Schematic pulse operation for two-pulse echoes.

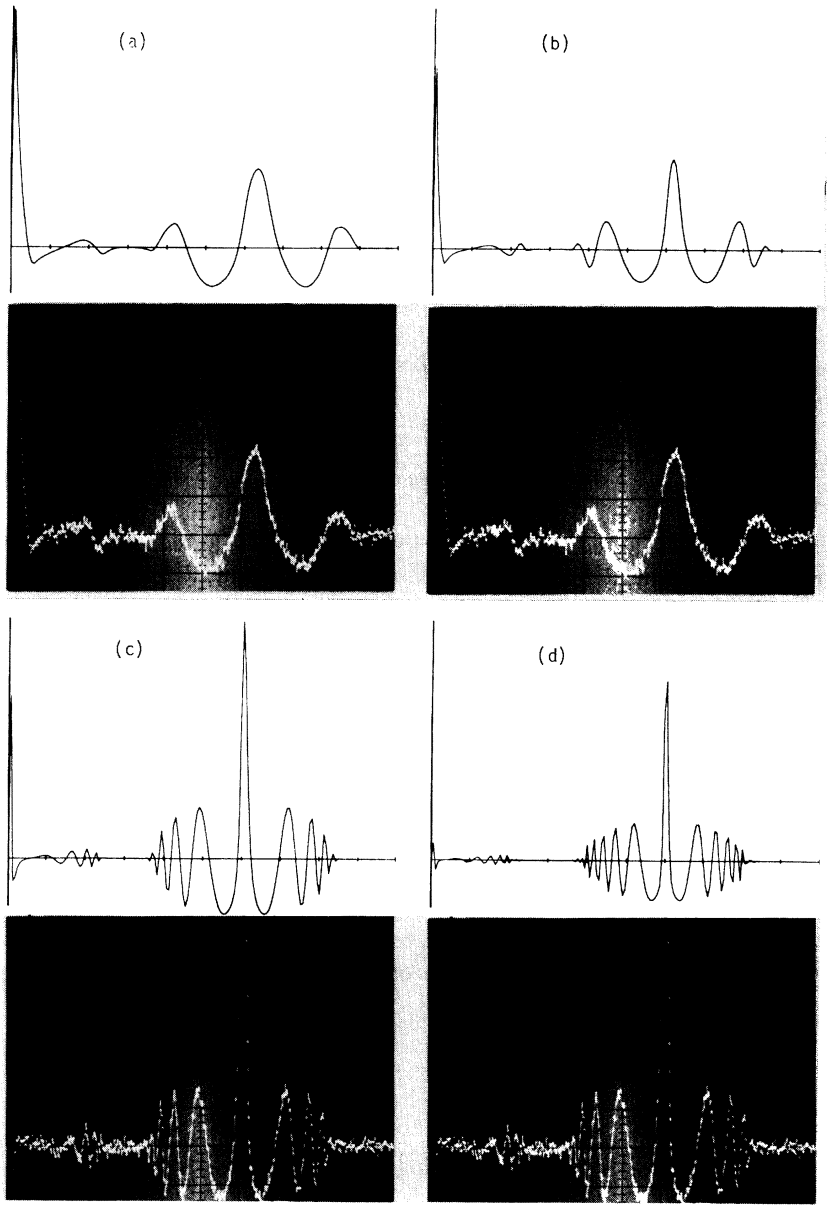

FIG. 5. Calculated and observed shapes of oscillatory spin-locked echo signals. The area of the second pulse is, from (a) to (d), 2π, 4π, 10π, and 20π. The horizontal scale is 250 μs/div.

give the echo. These echo terms coincide with Eq. (28) in Ref. 4 if the notations are altered. The shape of the echo is calculated by substituting (9) into (5), and results are shown in Figs. 5—8. Because $m_x(t)$ in this case is also an odd function of Δ, the u-mode signals vanishes as in the FID cases, when the line-shape function is symmetric about the center.

Generally, it is difficult to obtain analytic expressions of two-pulse echoes from Eq. (5). However, when σ^* is assumed to be infinite, analytic expressions can be obtained for the cases where only one of the pulses is a large-area one, as follows.

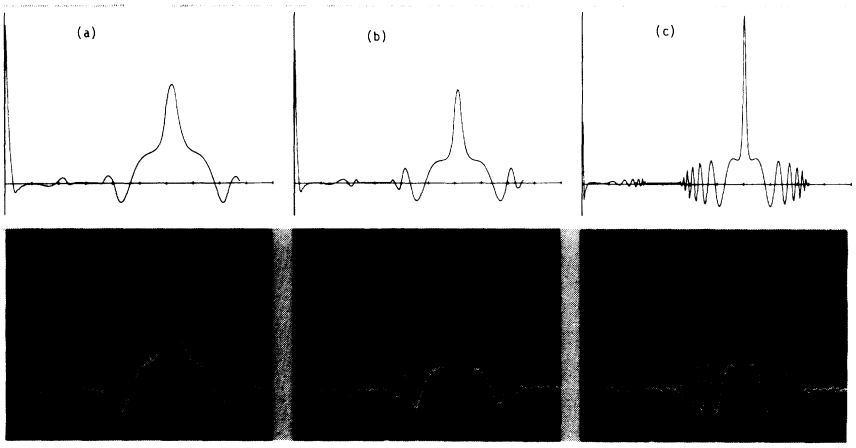

FIG. 6. Calculated and observed shapes of oscillatory spin-locked echo signals. The area of the second pulse is, from (a) to (c), 3π, 5π, and 15π. The horizontal scale is 250 μs/div.

1. *Locked-type echoes*

We first consider the case where only the area of the second pulse is large and the first pulse is so intense and short that the δ-function-type excitation can be assumed, i.e., the off-resonance effect during the first pulse and the duration τ_1 of the first pulse can be neglected. The off-resonance effect is taken into account only during the second pulse. We call the echoes obtained in this manner "locked-type echoes." In this case we obtain $m_y(t)$ after the second pulse ($t>\tau+\tau_2$) as

$$\begin{aligned} m_y/m_0=&-(1/\beta^2)(\cos\theta[\chi\Delta(1-\cos\beta\tau_2)\sin\Delta(t-\tau-\tau_2)-\chi\beta\sin\beta\tau_2\cos\Delta(t-\tau-\tau_2)] \\ &+\sin\theta\{\Delta\beta\sin\beta\tau_2\sin\Delta(t-\tau_2)-\tfrac{1}{2}[\chi^2+(\Delta^2+\beta^2)\cos\beta\tau_2]\cos\Delta(t-\tau_2\}) \\ &-(\tfrac{1}{2}\sin\theta)(\chi^2/\beta^2)(1-\cos\beta\tau_2)\cos\Delta(t-2\tau-\tau_2)\ , \end{aligned} \tag{10}$$

where θ is the area of the first pulse. The last term gives the echo.

When the linewidth σ^* is assumed to be infinite, the echo shape can be obtained by the following formula:

$$v(t)=-[\tfrac{1}{2}m_0\chi^2 g(0)\sin\theta]I(t)\ , \tag{11}$$

where

$$I(t)=\int_{-\infty}^{+\infty}(1/\beta^2)(1-\cos\beta\tau_2)\cos\Delta(t-2\tau-\tau_2)d\Delta\ . \tag{12}$$

The echo pattern is determined by the integral $I(t)$ independent of θ.

In order to evaluate the integral $I(t)$, we apply the Laplace transform in the variables p and τ_2 as

$$F(p)=\int_0^{\infty}I(\tau_2)\exp(-p\tau_2)d\tau_2=\mathscr{L}I(\tau_2)\ , \tag{13}$$

where the quantity $(t-2\tau-\tau_2)$ is held fixed. Performing the integration in τ_2, we obtain an explicit form of $F(p)$ as

$$F(p)=[\pi/p(p^2+\chi^2)^{1/2}]\exp[-|t-2\tau-\tau_2|(p^2+\chi^2)^{1/2}]\ . \tag{14}$$

If we put

$$F(p)=\pi G(p)/p\ , \tag{15}$$

the integral $I(t)$ becomes

$$I(t)=\mathscr{L}^{-1}F(p)=\pi\mathscr{L}^{-1}G(p)/p=\pi\int_0^{\tau_2}G(s)ds\ , \tag{16}$$

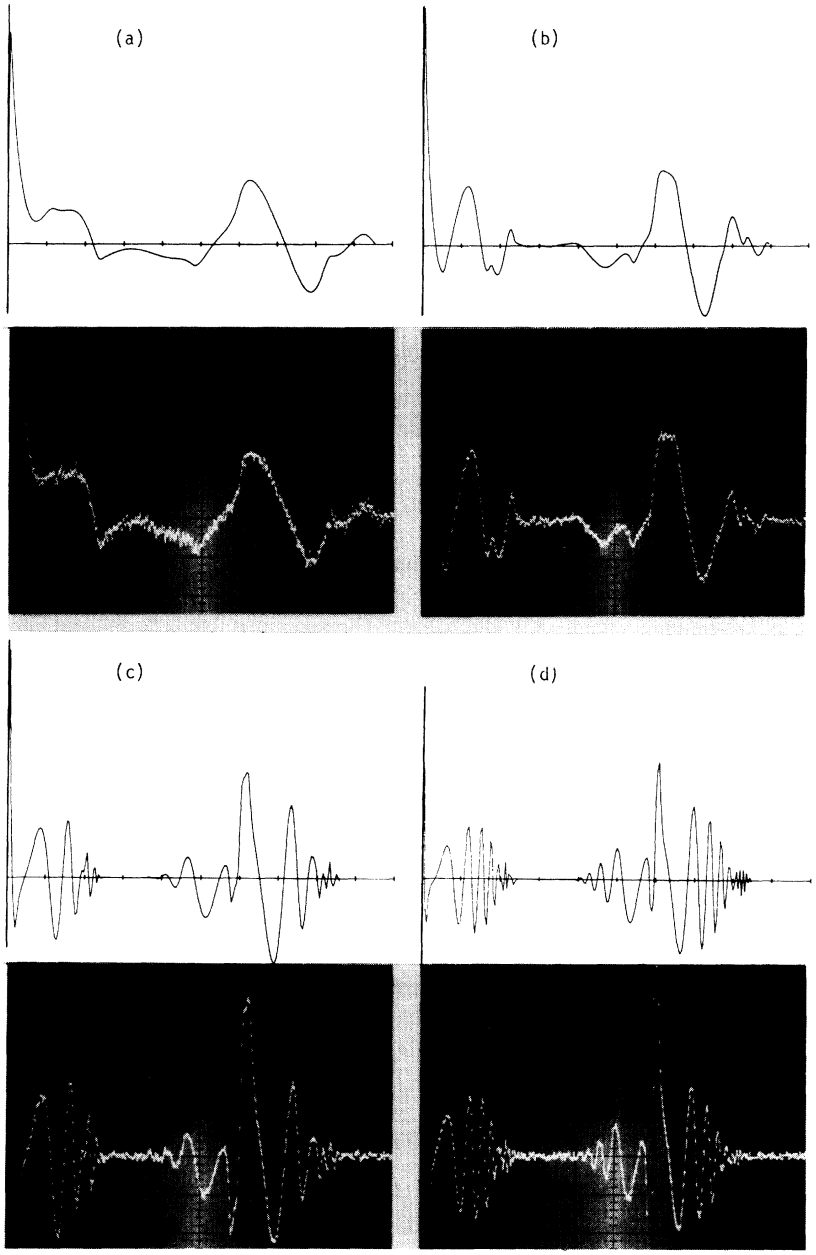

FIG. 7. Calculated and observed shapes of oscillatory notched echo signals. The area of the first pulse is, from (a) to (d), 2π, 4π, 10π, and 20π. The horizontal scale is 250 μs/div.

where

$$G(s)=\mathcal{L}^{-1}G(p)\ . \tag{17}$$

The inverse Laplace transform yields[9]

$$G(s)=\begin{cases}0, & 0<s<|t-2\tau-\tau_2| \\ J_0\{\chi[s^2-(t-2\tau-\tau_2)^2]^{1/2}\}, & s>|t-2\tau-\tau_2|\end{cases}\ . \tag{18}$$

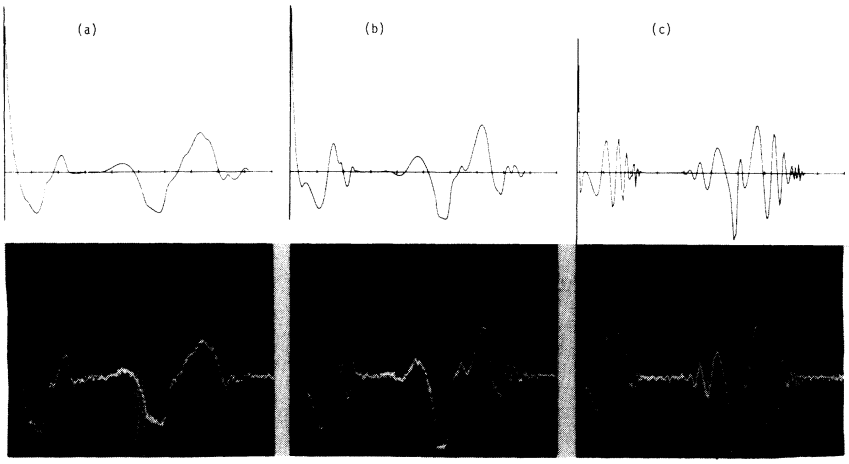

FIG. 8. Calculated and observed shapes of oscillatory notched echo shapes. The area of the first pulse is, from (a) to (c), 3π, 5π, and 15π. The horizontal scale is 250 μs/div.

From Eq. (18), $I(t)$ is obtained as

$$I(t)=\begin{cases}0, & t<2\tau \text{ and } t>2\tau+2\tau_2 \\ \pi\int_{|t-2\tau-\tau_2|}^{\tau_2} J_0\{\chi[s^2-(t-2\tau-\tau_2)^2]^{1/2}\}ds, & 2\tau<t<2\tau+2\tau_2\end{cases} \tag{19}$$

Equation (19) shows that the locked-type echoes display a uniform oscillation, which is symmetric about the center at $t=2\tau+\tau_2$, and the echo signal appears only for a time τ_2 before and after the echo center. These characteristics are similar to those of the oscillatory FID. The oscillation of the echo is also qualitatively understood as the sideband effect and the limited length of the echo is closely related to the theorem on coherent transients recently derived by SWB.[10] However, the oscillation pattern is different from that of FID. Instead of the Bessel function J_1 in the case of FID [Eq.(8)], J_0 appears in Eq. (19). In the case of FID, the large-area pulse is applied to the moments pointing along the z direction, whereas in the present case the large-area pulse is applied to the moments in the xy plane, whose directions are randomized by the inhomogeneous broadening. The locked-type echoes arise from the memory stored along the direction of the rf field (x axis). Echo shapes obtained from Eq. (19) are nearly the same as those obtained from numerical calculations using Eqs. (9) and (5), which are shown in Figs. 5 and 6.

2. *Notched-type echoes*

In this case, the area of the first pulse is large and the δ-function-type excitation is assumed for the second pulse. We call the echoes formed by this type of excitation "notched-type echoes." When the area of the second pulse is θ, a similar calculation gives $m_y(t)$ after the second pulse ($t>\tau_1+\tau$) as

$$\begin{aligned} m_y/m_0=(1/\beta^2)\{&\sin\theta(\Delta^2+\chi^2\cos\beta\tau_1)\cos\Delta(t-\tau_1-\tau) \\ &-(1+\cos\theta)(\chi/2)[\Delta(1-\cos\beta\tau_1)\sin\Delta(t-\tau_1)-\beta\sin\beta\tau_1\cos\Delta(t-\tau_1)]\} \\ &-[(1-\cos\theta)/2](\chi/\beta^2)[\Delta(1-\cos\beta\tau_1)\sin\Delta(t-\tau_1-2\tau)+\beta\sin\beta\tau_1\cos\Delta(t-\tau_1-2\tau)] . \end{aligned} \tag{20}$$

The last term gives the echo. Assuming $\sigma^*=\infty$, we obtain the expression corresponding to (11):

$$v(t)=-[\tfrac{1}{2}m_0(1-\cos\theta)\chi g(0)]I(t) , \tag{21}$$

where

$$I(t)=\int_{-\infty}^{\infty}(1/\beta^2)[\Delta(1-\cos\beta\tau_1)\sin\Delta(t-\tau_1-2\tau)+\beta\sin\beta\tau_1\cos\Delta(t-\tau_1-2\tau)]d\Delta\ . \tag{22}$$

The Laplace transform of $I(t)$ with $(t-\tau_1-2\tau)$ held fixed becomes

$$F(p)=\pi[\pm 1/p+1/(p^2+\chi^2)^{1/2}]\exp[-|t-\tau_1-2\tau|(p^2+\chi^2)^{1/2}]\ , \tag{23}$$

where the plus and the minus signs are adopted when $t-\tau_1-2\tau>0$ and $t-\tau_1-2\tau<0$, respectively. For $t<\tau_1+2\tau$, $I(t)$ is of the same form as in the case of FID[1] except for the minus sign. Therefore, $I(t)$ is obtained as

$$I(t)=\begin{cases}0, & t<2\tau\\ -\pi\chi\displaystyle\int_{|t-\tau_1-2\tau|}^{\tau_1}\left[\frac{s-(t-\tau_1-2\tau)}{s+(t-\tau_1-2\tau)}\right]^{1/2}J_1\{\chi[s^2-(t-\tau_1-2\tau)^2]^{1/2}\}ds, & 2\tau<t<\tau_1+2\tau\end{cases} \tag{24}$$

For $t>\tau_1+2\tau$, we divide $F(p)$ into two terms as

$$F(p)=\pi[1/p-1/(p^2+\chi^2)^{1/2}]\exp[-|t-\tau_1-2\tau|(p^2+\chi^2)^{1/2}]$$
$$+[2\pi/(p^2+\chi^2)^{1/2}]\exp[-|t-\tau_1-2\tau|(p^2+\chi^2)^{1/2}]\ . \tag{25}$$

The first term is of the same form as in the case of $t<\tau_1+2\tau$ except for the minus sign. The inverse transform of the second term is listed in the table of Ref. 9. Thus $I(t)$ becomes

$$I(t)=\begin{cases}0, & t>2\tau_1+2\tau\\ \pi\left[\chi\displaystyle\int_{t-\tau_1-2\tau}^{\tau_1}\left[\frac{s-(t-\tau_1-2\tau)}{s+(t-\tau_1-2\tau)}\right]^{1/2}J_1\{\chi[s^2-(t-\tau_1-2\tau)^2]^{1/2}\}ds\right.\\ \left.\quad+2J_0\{\chi[\tau_1^2-(t-\tau_1-2\tau)^2]^{1/2}\}\right], & \tau_1+2\tau<t<2\tau_1+2\tau\ .\end{cases} \tag{26}$$

Equations (24) and (26) show that the notched-type echoes display oscillations. However, in contrast to the oscillation in the locked-type echoes, the oscillation is neither uniform nor symmetric around the echo center at $t=\tau_1+2\tau$. If the second term in Eq. (26) was absent, the echo pattern would be antisymmetric about the echo center. The echo behavior can be qualitatively understood as follows: The second pulse gives rise to the effective time reversal in the motion of the moments. The echo pattern before the echo center reflects the time reversed motion after the first pulse which is represented by J_1 in Eq. (24). In the echo pattern after the echo center, however, the contribution of the time reversed motion during the first pulse, which is represented by J_0 in Eq. (26), are superposed on the former motion. Thus the pattern of the notched-type echoes become complicated.

The echo shape obtained from Eq. (26) shows discontinuity at $t=2\tau_1+2\tau$. This arises from the assumptions of the infinite linewidth and the δ-function-type excitation of the second pulse. Numerical calculations based on Eqs. (5) and (9), where both the linewidth and the pulse length are finite, give the echo shapes without discontinuity, which are in good agreement with the experimental results, as shown in Figs. 7 and 8. However, main characteristics of the notched-type echoes are represented by Eqs. (24) and (26). The discontinuity is due to the mathematical reason that the integrand in Eq. (22) is of the order of Δ^{-1}. The reason why the discontinuity is absent in the case of the locked-type echoes is that the integrand in Eq. (12) is inversely proportional to Δ^2.

III. EXPERIMENTAL DETAILS AND RESULTS

A. Apparatus and sample

NMR signals were detected by a homebuilt NMR spectrometer operating at 11.002 MHz. It provides various rf pulse sequences with variable amplitude and rf phase. Phase sensitive detection was used so that the u- and v-mode signals could be separately detected. The detected signals were

integrated and averaged by an averager (KAWASAKI ELECTRONICA TMC-400S) to observe the detailed structures of the oscillations of FID and echoes, which were in most cases, buried in the noise level.

The experiment was carried out on proton in water (~ 1 ml) which is a pure two-level spin system. In order to obtain a suitable length of the spin-lattice relaxation time T_1 for data collection, the water was doped by paramagnetic impurities (Cu^+ ions). The typical value of the homogeneous linewidth (FWHM) σ ($= 2/T_2$) estimated from the spin echo envelope decay time was $2\pi \times 85$ rad/s. The inhomogeneous linewidth (FWHM) σ^* was artificially increased by placing a piece of iron between the pole faces of the electromagnet. The resultant inhomogeneity across the sample was approximately 20 Oe. The shape of the inhomogeneous broadening was measured by plotting the amplitude of the spin echo signals versus H_0. The magnitude of H_1 of the rf field was measured from the length of a $\pi/2$ pulse and was adjusted so that the condition $\sigma^* > \chi > \sigma$ was satisfied. An operation to observe FID or echo signal was finished in a time much shorter than T_2 and therefore the effect of T_2 (and also that of T_1 which was approximately equal to T_2) could be neglected.

B. Free-induction decay

Oscillatory FID signals observed for

$$\chi\tau_1 = 2n\pi \quad (n = 1,2,5,10,15,20)$$

are shown in Figs. 1 and 2, together with the results of numerical calculations using Eqs. (7) and (5). These are the v-mode signals. The reference signal of the phase sensitive detector was adjusted to be in phase with respect to FID obtained by a $\pi/2$ pulse. The pulse area $\chi\tau_1$ was changed by changing the rf field intensity H_1 and keeping the pulse duration τ_1 fixed ($\simeq 0.6$ ms). The vertical scale was normalized on the oscilloscope so that the observed amplitude of the first oscillation was equal to that of the calculated one. All signals in Figs. 1 and 2 were obtained by integrating 128 times.

Agreements between observed signals and calculated curves are quite excellent. If one put the former upon the latter, one finds them to coincide with each other except for the initial transient. The theory by SWB shows that the shape of the initial transient depends strongly on the shape of the inhomogeneous broadening. The observed shape of the inhomogeneous broadening in the present experiment was Gaussian-like but slightly asymmetric about the center. Discrepancies between observed and calculated initial transients are due to this asymmetry.

All characteristics of the oscillatory FID predicted by SWB[1] have been confirmed experimentally, which are (1) the oscillation frequency is, in first approximation, equal to the nutation frequency (Rabi frequency), (2) the FID signal following the pulse continues for a time as long as the pulse duration, (3) the number of oscillation increases by increasing the pulse area and the number of periods is almost equal to the number of nutation of the resonant dipoles around the driving field, and (4) the envelope of oscillation is approximately a linearly decreasing function of time.

In Fig. 3 observed and calculated FID signals for

$$\chi\tau_1 = (2n+1)\pi \quad (n = 1,2,7)$$

are shown. In these cases the oscillation is not uniform immediately after the initial transient. When the pulse area was increased by π, the oscillation became uniform. Agreements between experiment and calculation are also excellent.

We also examined the characteristics of FID when the pulse area was changed by changing the duration τ_1, instead of changing χ, and keeping the value of χ fixed. The observed signals also behaved as the theory predicted. However, for the large pulse area, the observed amplitude was smaller than the calculated one due to the relaxation effect.

We also observed the u-mode signals arose from the asymmetry of the inhomogeneous broadening. They were small and sharp transients immediately after the pulse. The shape of these signals agreed with the calculated ones obtained by the asymmetric line shape function.

C. Two-pulse echoes

1. Locked-type echoes

Observed spin-locked echoes for

$$\chi\tau_2 = 2n\pi \quad (n = 1,2,5,10)$$

are shown in Fig. 5 together with theoretical curves obtained by the numerical calculations based on Eqs. (9) and (5). The first pulse was

made a $\pi/2$ pulse for obtaining maximum amplitude. The spacing τ between the pulses and the duration τ_2 of the second pulse were about 1.5 and 0.6 ms, respectively. The pulse area was changed by changing χ. The signals are the v-mode ones detected the same way as in the FID case, but the integration was done 512 times because of rather poor signal-to-noise ratio. Good oscillations appear on either side of the echo center, and are symmetric about the center. Agreements between observed and calculated shapes are satisfactory except for slight discrepancies in the vicinity of the center. This discrepancy is due to the asymmetry of the inhomogeneous broadening. Spin-locked echoes for

$$\chi\tau_2=(2n+1)\pi \quad (n=1,2,7)$$

are shown in Fig. 6. The oscillation patterns near the echo center are different from those in Fig. 5. Pedestal-like shapes appear near the center. These correspond to the FID shape immediately after the initial transient in the cases of $\chi\tau_1=(2n+1)\pi$. The observed and calculated shapes coincide with each other except for the part in the vicinity of the echo center as in Fig. 5. When the u-mode detection was performed, a small signal appeared near the echo center due to the asymmetry of the inhomogeneous broadening.

2. *Notched-type echoes*

Oscilloscope traces of the notched-type echoes for

$$\chi\tau_1=2n\pi \quad (n=1,2,5,10)$$

are shown in Fig. 7 together with calculated curves. The second pulse was made a π pulse. The spacing τ between the pulses and the duration τ_1 of the first pulse were 1.5 and 0.6 ms, respectively. The echoes are not symmetric about the echo center as is expected. Although the shapes are rather complicated, the observed signals successfully agree with the calculated ones. A small discrepancy due to the asymmetry of the inhomogeneous broadening appears in the neighborhood of the echo center. The oscillation on the left-hand side of the center is nearly the time-reversed pattern of the FID oscillation after the first pulse. Notched-type echoes for

$$\chi\tau_1=(2n+1)\pi \quad (n=1,2,7)$$

are shown in Fig. 8. The observed shapes also show very good agreement with the calculated ones. The echoes in Figs. 7 and 8 vanished in the u-mode detection, leaving very small signal about the echo center.

IV. CONCLUDING REMARK

Oscillatory FID theoretically predicted by SWB was confirmed experimentally by using NMR in an inhomogeneously broadened proton system. Oscillatory echoes were also observed in the same system in the cases of spin-locked and notched echoes. Behaviors of these echoes were found to be fully explained by the Bloch equations. We are now studying theoretically and experimentally on two-pulse echoes in general cases and have found analytic expressions of the echo shapes produced by two pulses with arbitrary amplitude and duration. Details will be reported in the near future. It is interesting to study oscillatory FID and echoes in optical-resonance experiments. The present work should provide a basis for such studies.

[1]A. Schenzle, N. C. Wong, and R. G. Brewer, Phys. Rev. A 21, 887 (1980).
[2]M. Kunitomo, T. Endo, S. Nakanishi, and T. Hashi, Phys. Lett. 80A, 84 (1980).
[3]T. Endo, S. Nakanishi, T. Muramoto, and T. Hashi, Opt. Commun. 37, 369 (1981).
[4]A. L. Bloom, Phys. Rev. 98, 1105 (1955).
[5]W. B. Mims, Phys. Rev. 141, 499 (1966).
[6]S. R. Hartmann and E. L. Hahn, Phys. Rev. 128, 2042 (1962).
[7]P. F. Liao and S. R. Hartmann, Phys. Lett. 44A, 361 (1973).
[8]M. Kunitomo and T. Hashi, Phys. Lett. 81A, 299 (1981).
[9]H. Bateman, *Tables of Integral Transforms* (McGraw-Hill, New York, 1954).
[10]A. Schenzle, N. C. Wong, and R. G. Brewer, Phys. Rev. A 22, 635 (1980).

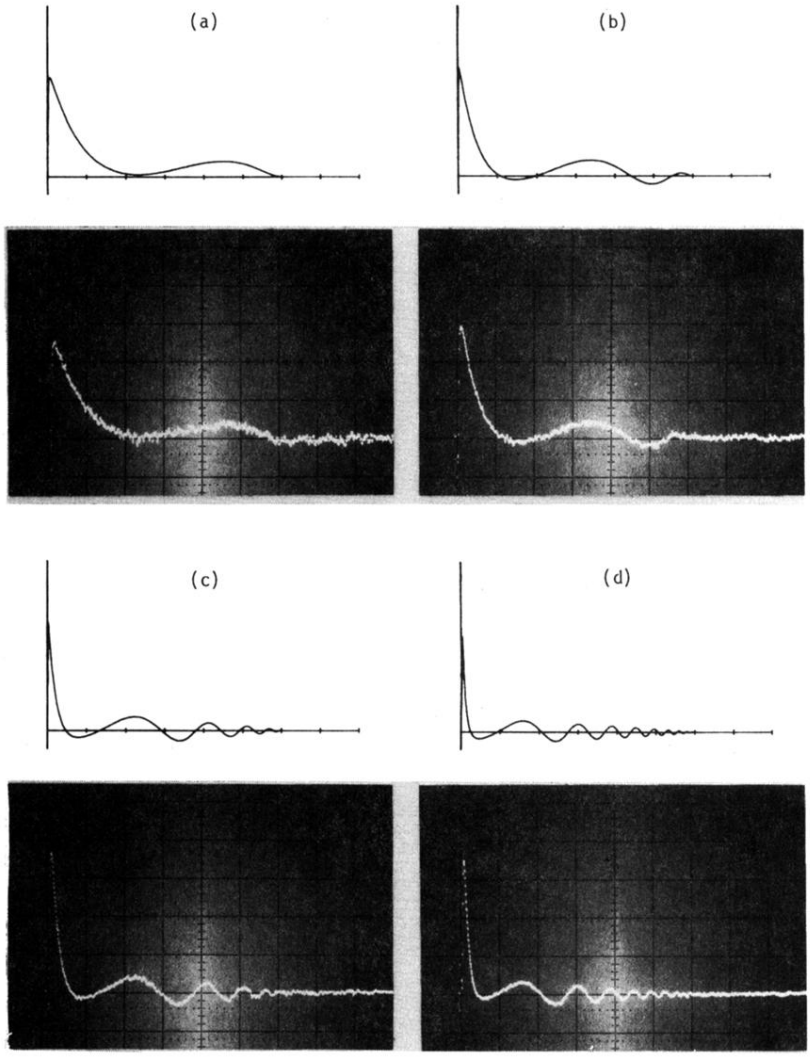

FIG. 1. Calculated and observed shapes of oscillatory FID signals for pulse area 2π, 4π, 10π, and 20π [from (a) to (d)]. The horizontal scale is 100 μs/div.

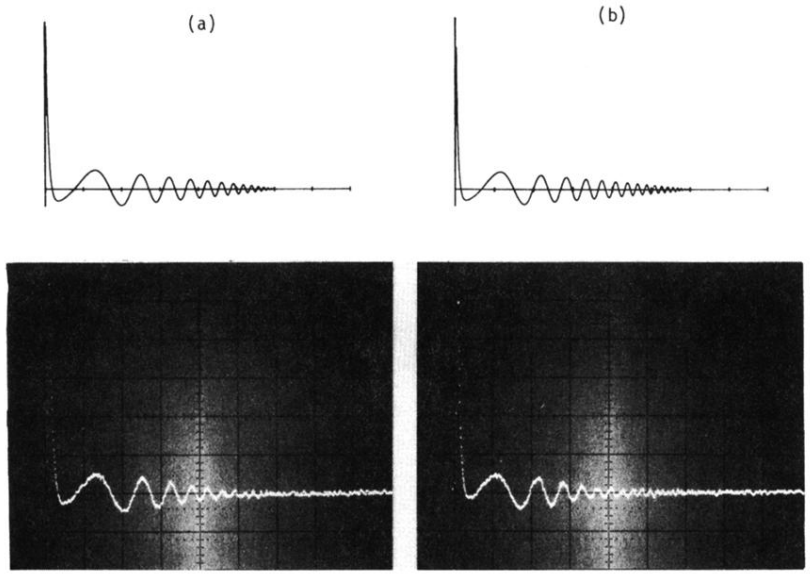

FIG. 2. Calculated and observed shapes of oscillatory FID signals for pulse area (a) 30π and (b) 40π. The horizontal scale is 100 μs/div.

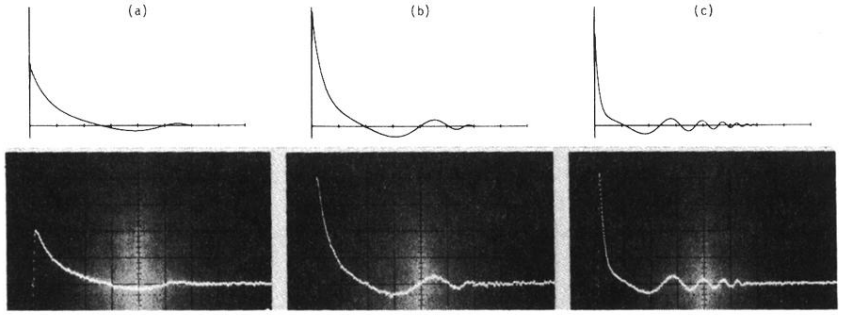

FIG. 3. Calculated and observed shapes of oscillatory FID signals for pulse area 3π, 5π, and 15π [from (a) to (c)]. The horizontal scale is 100 μs/div.

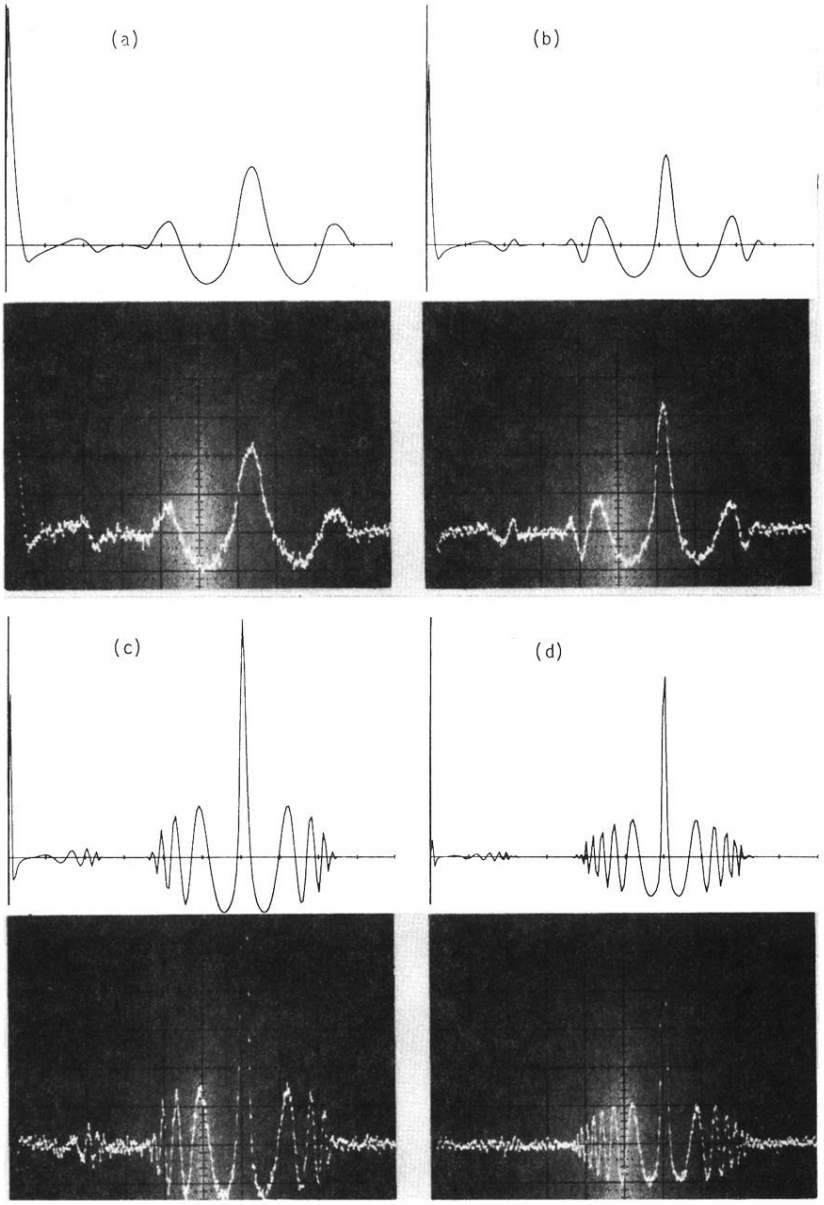

FIG. 5. Calculated and observed shapes of oscillatory spin-locked echo signals. The area of the second pulse is, from (a) to (d), 2π, 4π, 10π, and 20π. The horizontal scale is 250 μs/div.

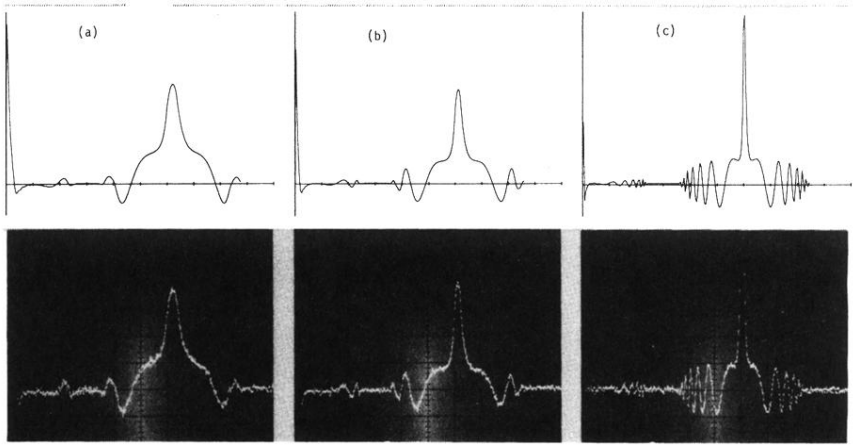

FIG. 6. Calculated and observed shapes of oscillatory spin-locked echo signals. The area of the second pulse is, from (a) to (c), 3π, 5π, and 15π. The horizontal scale is 250 μs/div.

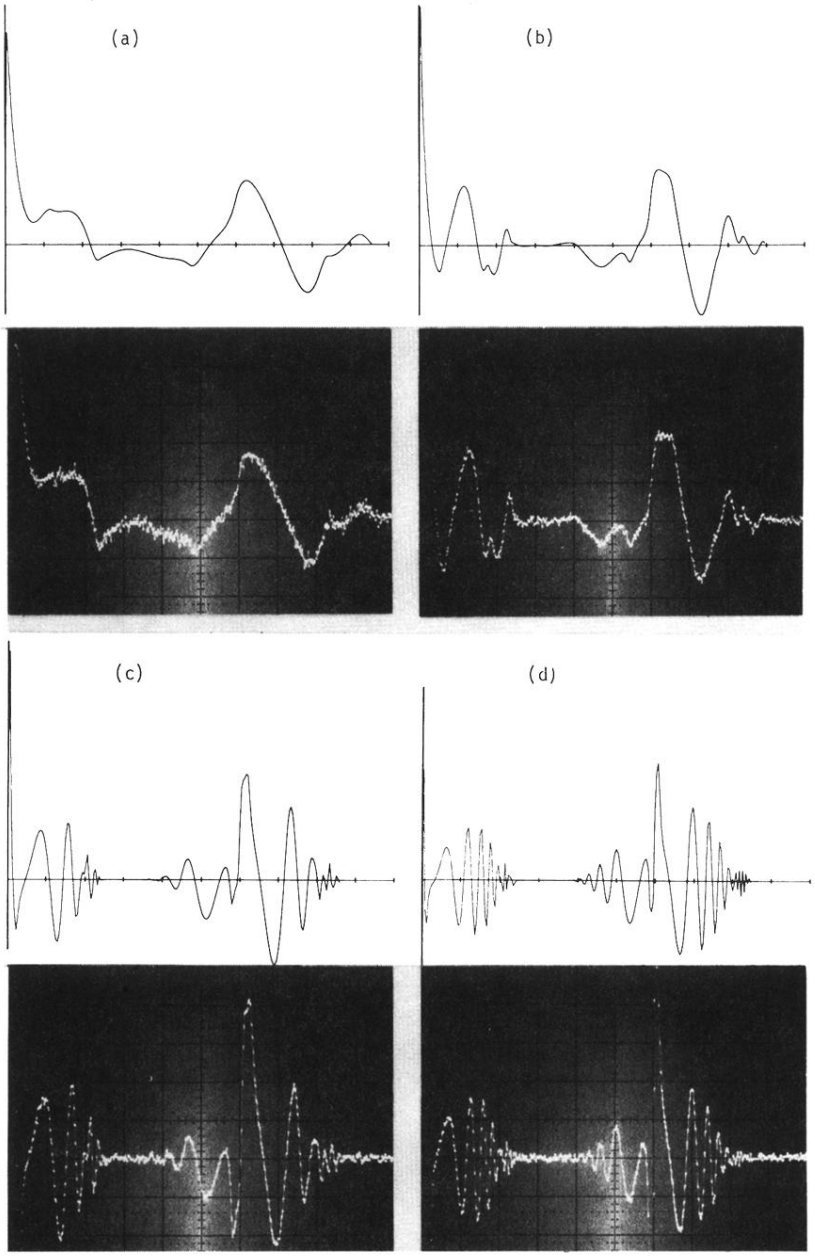

FIG. 7. Calculated and observed shapes of oscillatory notched echo signals. The area of the first pulse is, from (a) to (d), 2π, 4π, 10π, and 20π. The horizontal scale is 250 μs/div.

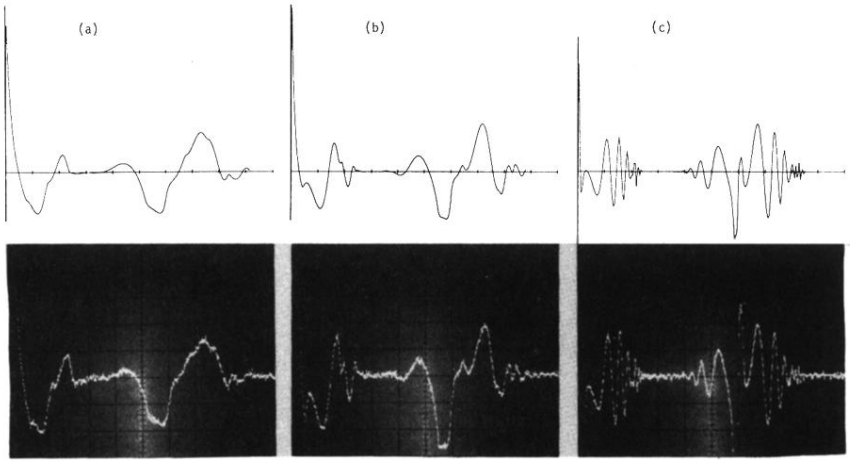

FIG. 8. Calculated and observed shapes of oscillatory notched echo shapes. The area of the first pulse is, from (a) to (c), 3π, 5π, and 15π. The horizontal scale is 250 μs/div.